Imaging the Magnetic Spin Structure of Exchange-Coupled Thin Films

R. Röhlsberger,[1,*] H. Thomas,[1] K. Schlage,[1] E. Burkel,[1] O. Leupold,[2] and R. Rüffer[2]

[1]*Fachbereich Physik, Universität Rostock, August-Bebel-Strasse 55, 18055 Rostock, Germany*

[2]*European Synchrotron Radiation Facility, BP 220, 38043 Grenoble Cedex, France*

(Received 31 May 2002; published 13 November 2002)

We have investigated the magnetic spin structure of a soft-magnetic film that is exchange-coupled to a hard-magnetic layer to form an exchange-spring layer system. The depth dependence of the magnetization direction was determined by nuclear resonant scattering of synchrotron radiation from ultrathin ^{57}Fe probe layers. In an external field a magnetic spiral structure forms that can be described within a one-dimensional micromagnetical model. The experimental method allows one to image vertical spin structures in stratified media with unprecedented accuracy.

DOI: 10.1103/PhysRevLett.89.237201 PACS numbers: 75.70.–i, 61.10.–i, 75.25.+z, 76.80.+y

The exchange coupling between different magnetic phases within thin films, multilayers, and nanoparticles plays an important role in the development of novel functional magnetic nanostructures. Applications include magnetoelectronic devices that are based on the exchange bias effect [1] and magnetostrictive heterostructures in micromechanical devices [2], for example. The functionality of these systems relies critically on the magnetic spin structure that develops in external magnetic fields [3]. Moreover, nanocomposite materials consisting of exchange-coupled soft- and hard-magnetic phases are promising candidates for new permanent magnetic materials with giant magnetic energy products [4]. Thin bilayers consisting of a hard- and a soft-magnetic material are ideal model systems to investigate the fundamental properties of this coupling mechanism. As a characteristic property of such systems, the magnetization of the soft-magnetic film at the interface is pinned to the hard-magnetic film as a result of the exchange interaction. With increasing distance from the interface, the exchange coupling becomes weaker and the magnetization may rotate under the action of an external field. If, for example, the external field is applied orthogonal to the magnetization direction of the hard layer, the magnetic moments in the soft layer arrange in a spiral structure along the normal, as shown schematically in Fig. 1. Because of the reversible nature of this rotation, this is called the exchange-spring effect [5]. While a number of micromagnetical models have been developed to describe this behavior [6,7], direct measurements of the actual spin structure are scarce. Methods applied so far such as polarized neutron scattering either probe the whole volume of the sample or they are too surface sensitive as in case of electron scattering. In the former case, however, special reconstruction techniques allow one to extract depth-resolved spin structures as demonstrated recently [8]. In the past, conversion electron Mössbauer spectroscopy was applied to study the depth dependence of magnetic properties in thin films via selectively deposited ^{57}Fe monolayer probes [9]. While measurements in this field are time-consuming even with the use of strong radioactive sources, the availability of high-brilliance synchrotron radiation has opened new avenues for the study of thin films and low-dimensional structures [10,11], involving ultrathin probe layers as well.

In this Letter we report about the direct measurement of the depth-dependent spin rotation in exchange-coupled bilayers consisting of Fe on hard-magnetic FePt with unidirectional magnetization, as shown in Fig. 1. The experimental method is coherent nuclear resonant scattering of synchrotron radiation from ^{57}Fe probe layers in different depths within the Fe layer. The simultaneous excitation of the hyperfine-split nuclear energy levels leads to characteristic beats in the time spectra of the nuclear decay from which the magnitude and the orientation of magnetic fields in the sample can be determined with high accuracy. The method is the time-based analog of classical Mössbauer spectroscopy that was introduced as nuclear Bragg scattering by Gerdau *et al.* [12] and

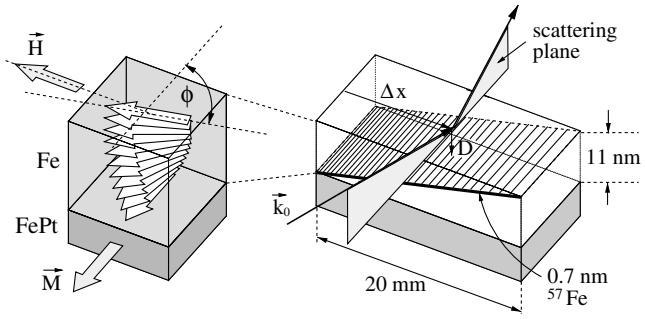

FIG. 1. Left: scheme of the spin structure in an exchange-spring bilayer consisting of a soft-magnetic layer (Fe) on a hard-magnetic layer (FePt) with uniaxial anisotropy. An external field $\vec{H}$ is applied perpendicular to the remanent magnetization $\vec{M}$ of the hard layer. Right: to image the resulting magnetic spiral, a tilted ultrathin probe layer of ^{57}Fe is deposited within the soft layer. The magnetic properties in depth D of the film are probed by adjusting the transverse displacement Δx of the sample relative to the scattering plane.

extended to nuclear forward scattering (NFS) by Hastings *et al.* [13,14].

The sample investigated here is a bilayer system consisting of 11 nm Fe on 30 nm $Fe_{55}Pt_{45}$, further denoted as FePt. The layers were deposited by rf magnetron sputtering in an Ar atmosphere of 1.5×10^{-2} mbar on a superpolished Si wafer. FePt was sputtered from a composite target consisting of a number of Pt chips on a high-purity Fe foil to obtain the desired composition. After deposition, the layer was annealed for 30 min at 800 K to form the hard-magnetic tetragonal $L1_0$ phase [15,16] with a coercivity of 0.96 T at room temperature, as controlled by hysteresis measurements via the magneto-optical Kerr effect. The rms surface roughness of the FePt layer was determined by x-ray reflectivity to be less than 0.4 nm, indicating that the grain size did not increase too much upon annealing. To prepare a tilted probe layer within the Fe film, as shown schematically in Fig. 1, a wedge-shaped film with a slope of 0.5 nm/mm is produced by linear variation of the exposure during sputter deposition of Fe. After growth of a 0.7 nm thick ^{57}Fe probe layer the same wedge was deposited with opposite slope. Different depths D in the sample can thus be probed by adjusting the displacement Δx of the sample transversely to the incident beam. Finally, the layer system was coated with 3 nm Ag to minimize oxidation.

The experiment was performed in the single-bunch filling mode of operation at the Nuclear Resonance beam line (ID18) of the European Synchrotron Radiation Facility [17]. At the sample position the beam cross section was 150 μm (vertical) $\times$ 200 μm (horizontal). The sample was magnetically saturated in an external field of 2.3 T so that the remanent magnetization of the FePt layer was oriented along $\vec{k}_0$, as shown in Fig. 1. It was mounted in a cryomagnet system with an in-plane external field perpendicular to $\vec{k}_0$ where it was cooled to 4 K to increase the coercivity and the remanence of the hard-magnetic layer [18]. To maximize the delayed intensity, the radiation was coupled into a waveguide mode of the layer system at an angle of incidence of $\varphi_m \approx \sqrt{\varphi_c^2 + \lambda^2/16d^2} = 4.4$ mrad, where $\varphi_c = 3.8$ mrad is the critical angle of Fe and d is the Fe layer thickness. This is illustrated in Fig. 2. The superposition of waves that are multiply reflected at the Ag/Fe/FePt boundaries led to a significant x-ray flux enhancement inside the Fe layer, shown in Fig. 2(a). At $\varphi = \varphi_m$ we have observed a maximum resonant (delayed) count rate of about 100 s^{-1}, see Fig. 2(c), so that time spectra with very good statistical quality were obtained within only 15 min. A series of time spectra taken at selected transverse displacements Δx and external magnetic fields B is shown in Fig. 4. The beat pattern in the spectra undergoes characteristic changes that reflect the rotation of the magnetization, as will be discussed in detail below.

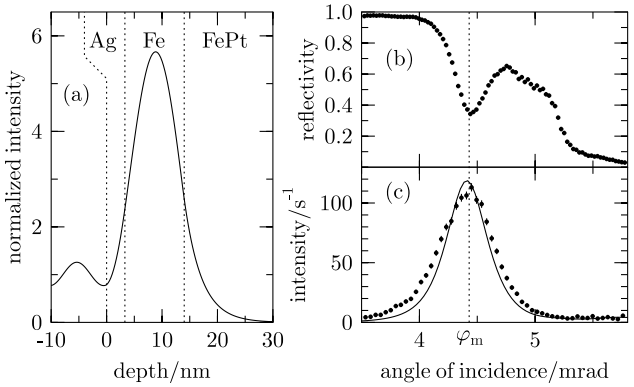

FIG. 2. The Ag/Fe/FePt trilayer as an x-ray waveguide. (a) Depth dependence of the electric field intensity at an angle of incidence of $\varphi_m = 4.4$ mrad. At this angle, the radiation couples into a guided mode, forming a standing wave inside the Fe layer. This shows up as a minimum in the rocking curve of the nonresonant reflectivity (b) and as a pronounced peak in the flux of the resonantly scattered radiation (c), recorded within a time range from 20–160 ns after excitation.

Because of the very small thickness of the probe layer we can describe the delayed temporal response in the kinematical approximation of NFS. In this case the amplitude of the resonantly scattered radiation is proportional to the nuclear scattering amplitude $f(\omega)$. The 14.4 keV transition of ^{57}Fe is a magnetic dipole transition with spins $I_g = 1/2, I_e = 3/2$ of the ground and the excited state, respectively, and a natural lifetime of $\tau_0 = 141$ ns. Since in this scattering geometry the magnetic field of the incident radiation is along the surface normal, and the magnetization lies in the plane of the sample, only transitions with a change in the magnetic quantum number of $\Delta m = \pm 1$ can be excited. Assuming detection without polarization analysis, the time dependence of the resonantly reflected intensity is given by [19]

$$I(t) = |(\tilde{F}_{+1} + \tilde{F}_{-1}) + i\cos\phi(\tilde{F}_{+1} - \tilde{F}_{-1})|^2 e^{-\chi t/\tau_0}, \quad (1)$$

where the functions $\tilde{F}_\nu = \tilde{F}_\nu(t)$ are the Fourier transforms of the energy-dependent resonant strengths $F_\nu(\omega)$ for dipole transitions with a change in the magnetic quantum number of $\Delta m = \nu$, shown in Fig. 3(a). The exponential in Eq. (1) describes the acceleration of the decay that results from the coherent nature of the resonant scattering process [14]. At $\phi = 0$, Eq. (1) simplifies to $I(t) \sim |\tilde{F}_{+1}|^2 + |\tilde{F}_{-1}|^2$. Since $|\tilde{F}_{+1}|^2 = |\tilde{F}_{-1}|^2$, the time spectrum $I(t)$ is a beat pattern with a single frequency (see Fig. 4, bottom right), reflecting the energetic separation of the two resonance lines that comprise the $F_\nu(\omega)$. With increasing ϕ the modulation becomes more complex due to the admixture of three more frequencies and merges into $I(t) \sim |\tilde{F}_{+1} + \tilde{F}_{-1}|^2$ at $\phi = 90°$. This behavior can be observed in Fig. 4: With increasing Δx the time spectra probe the Fe layer from the FePt interface up to the Ag interface. From the fit of the measured data according to Eq. (1) the planar rotation angle ϕ of the

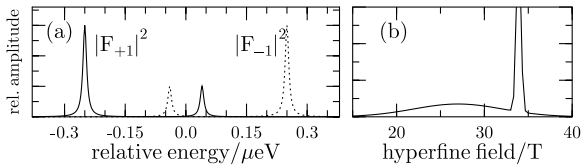

FIG. 3. (a) Modulus squared of the energy-dependent resonant strengths $F_{+1}(\omega)$ (solid line) and $F_{-1}(\omega)$ (dashed line) for the 14.4 keV transition in ferromagnetic ^{57}Fe. (b) Hyperfine field distribution that was used to simulate the time spectra of the probe layer close to the Fe/Ag interface.

magnetization in depth D of the Fe layer was derived, with the magnetic hyperfine field given by $B = 33.8$ T. At $\Delta x = 2$ mm the magnetization is aligned close to the FePt magnetization while at $\Delta x = 18$ mm the magnetic hyperfine field is almost parallel to the external field. The evolution of the magnetization rotation between these positions is plotted in Fig. 5. Data were recorded for external fields of $H = 160$, 240, and 500 mT, all within the reversibility range of the hysteresis loop. With increasing external field greater parts of the Fe film become aligned towards the external field. We have simulated this behavior by application of a one-dimensional micromagnetic model [6]. The layer system is divided into N sublayers of thickness $d = (d_{\mathrm{Fe}} + d_{\mathrm{FePt}})/N$. The total magnetic energy of this layer system is given by the sum of the magnetic exchange and anisotropy energies and the dipolar interaction with the external field, respectively:

$$E = -\sum_{i=1}^{N-1} \frac{A_{i,i+1}}{d^2} \cos(\phi_i - \phi_{i+1}) - \sum_{i=1}^{N} K_i \cos^2 \phi_i - \sum_{i=1}^{N} H M_i \cos(\phi_i - \phi_H). \quad (2)$$

In this experiment the external field H is oriented at an angle $\phi_H = \pi/2$ relative to the hard axis given by $\vec{M}$. $A_{i,i+1}$ is the exchange constant between sublayers i and $i+1$, K_i is the anisotropy constant, and M_i is the magnetization of the ith sublayer. To find the equilibrium spin configuration, the magnetic energy has to be minimized for each of the ϕ_i. For a given sublayer i the new orientation ϕ_i is determined from the condition $\partial E/\partial \phi_i = 0$. This procedure is repeated all over until equilibrium for all sublayers is reached. The solid lines in Fig. 5 are the results of the simulation showing a reasonable agreement with the measured data. For the FePt layer we have used the parameters $K_h = 4.0 \times 10^7$ erg/cm^3, $M_h = 1100$ emu/cm^3, and $A_h = 1.0 \times 10^{-6}$ erg/cm, as given in [20]. For the Fe layer we have assumed $K_s = 1.0 \times 10^3$ erg/cm^3, $M_s = 1900$ emu/cm^3, and $A_s = 1.0 \times 10^{-6}$ erg/cm. For the exchange constant at the interface we have assumed $A_{\mathrm{int}} = (A_h + A_s)/2$. The anisotropy constant K_s was estimated from the coercivity of a single Fe layer. Because of the polycrystalline nature

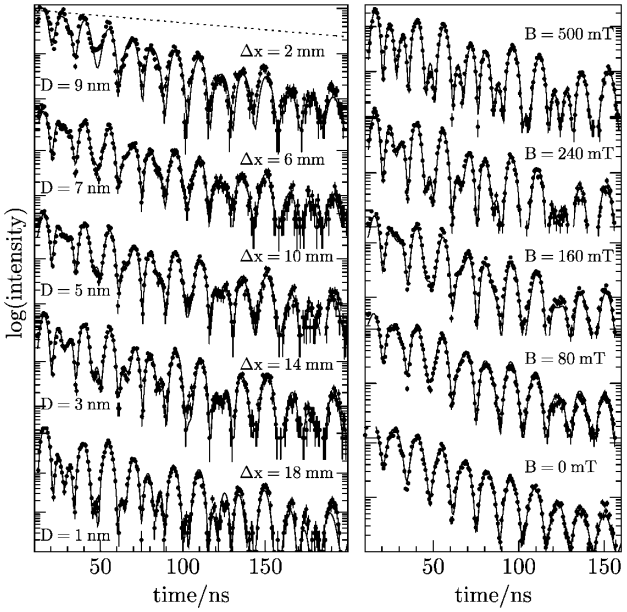

FIG. 4. Measured time spectra of grazing incidence reflection. Left: variation of the lateral positions Δx in a perpendicular magnetic field of $B = 160$ mT. Right: variation of the external magnetic field at $\Delta x = 10$ mm, where the ^{57}Fe probe layer is in the center of the Fe layer. In each case the change in the beat pattern reflects the rotation of the magnetization direction. Solid lines are theoretical simulations according to Eq. (1). The rotation angles derived from the simulations are shown in Fig. 5.

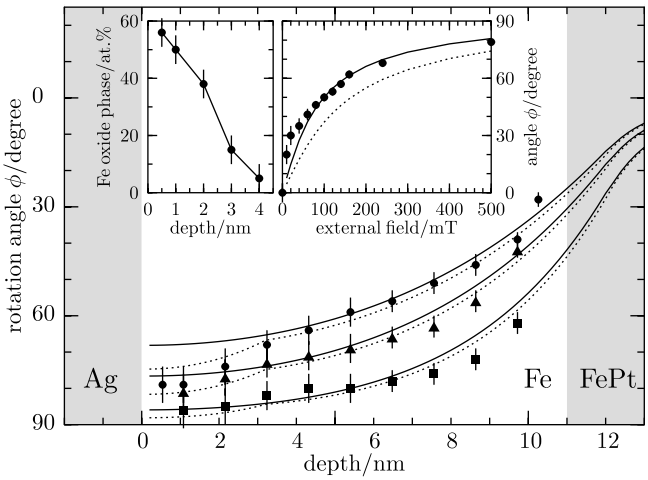

FIG. 5. Depth dependence of the spin rotation in the Fe layer for external magnetic fields of 160 mT (•), 240 mT (▲), and 500 mT (■). Shaded regions mark the Ag capping layer and the FePt substrate, respectively. Solid lines are simulations according to the model outlined in the text. The dashed lines are simulations assuming a reduced exchange coupling in the first 3 nm of the Fe layer. The left inset shows the depth dependence of the Fe oxide phase, given in at.%. The right inset displays the rotation angle in the center of the Fe layer as a function of the external magnetic field with simulations for $A_s = 1.0 \times 10^{-6}$ erg/cm (solid line) and $A_s = 2.8 \times 10^{-6}$ erg/cm (dashed line).

of the Fe layer the volume anisotropy becomes negligible, resulting in an anisotropy constant that is more than 2 orders of magnitude smaller than the bulk value [6]. The exchange constant A_s of the Fe layer was the only parameter that had to be adjusted in the simulation procedure [21]. Very likely, A_s depends on the microstructure of the film that is determined by the deposition process. In regions close to the top of the Fe layer the measured rotation angle deviates significantly from the simulations. The dashed lines are simulations under the assumption that the exchange constant is reduced to $A_s = 3.0 \times 10^{-7}$ erg/cm in the top 3 nm of the Fe layer. This may be due to diffusion of oxygen through the Ag and the formation of a native Fe oxide. The hyperfine field distribution used to simulate the time spectrum at $\Delta x =$ 18 mm is shown in Fig. 3(b). The broad component around 27 T (a Gaussian with $\sigma = 5$ T) is characteristic for a native Fe oxide [23], which is to a great part ferromagnetic and aligned collinear to the magnetization of the Fe [24]. From the evaluation of the time spectra we obtain a decreasing fraction of the oxide phase with increasing distance from the Ag/Fe boundary, as shown in the left inset of Fig. 5. To confirm the validity of our model, we have recorded time spectra from the center of the Fe layer ($\Delta x = 10$ mm) as a function of the external field, shown in the right column of Fig. 4. The field dependence of the rotation angle ϕ is shown in the right inset of Fig. 5. The simulation (solid line) demonstrates the significance of the exchange constant of the soft layer as the relevant parameter for the exchange-spring behavior in this system. For comparison, the dashed line represents the simulation for an exchange constant of $A_s = 2.8 \times 10^{-6}$ erg/cm as given in [6]. The remaining discrepancies are most likely due to the formation of magnetic domains at low fields.

In summary, we have measured the vertical magnetic structure of an exchange-coupled bilayer system via nuclear resonant x-ray scattering. The use of ultrathin probe layers of the resonant isotope allows for a direct determination of the magnetic properties with a spatial resolution below 1 nm. The intensity enhancement due to x-ray interference effects allows for very short data acquisition times of a few minutes at modern synchrotron radiation sources. It is an intrinsic advantage of this technique that isotopic probe layers do not disturb the electronic and magnetic configuration of the system. The method can also be applied to Mössbauer isotopes such as ^{149}Sm, ^{161}Dy, and ^{151}Eu, for example, that are particularly interesting as constituents of new magnetic materials.

We gratefully acknowledge the support of P. Becker, PTB Braunschweig, and A. Bernhard during preparation of the experiments. Moreover, we thank M. Getzlaff and W. Drube for characterization of the samples. This work was supported by the German BMBF under Contract No. 05 KS1HRA/8.

*Electronic address: roehle@physik1.uni-rostock.de

[1] J. Nogués and I. K. Schuller, J. Magn. Magn. Mater. **192**, 203 (1999).
[2] A. Ludwig and E. Quandt, J. Appl. Phys. **87**, 4691 (2000).
[3] K. Mibu, T. Nagahama, T. Shinjo, and T. Ono, Phys. Rev. B **58**, 6442 (1998).
[4] R. Skomski and J. M. D. Coey, Phys. Rev. B **48**, 15812 (1993).
[5] E. F. Kneller and R. Hawig, IEEE Trans. Magn. **27**, 3588 (1991).
[6] E. E. Fullerton, J. S. Jiang, M. Grimsditch, C. H. Sowers, and S. D. Bader, Phys. Rev. B **58**, 12193 (1998).
[7] J. S. Jiang, H. G. Kaper, and G. K. Leaf, Discrete Contin. Dynam. Syst. Ser. B **1**, 219 (2001).
[8] K. V. O'Donovan, J. A. Borchers, C. F. Majkrzak, O. Hellwig, and E. E. Fullerton, Phys. Rev. Lett. **88**, 067201 (2002).
[9] J. Tyson, A. H. Owens, J. C. Walker, and G. Bayreuther, J. Appl. Phys. **52**, 2487 (1981); J. Korecki and U. Gradmann, Phys. Rev. Lett. **55**, 2491 (1985); G. Lugert and G. Bayreuther, Phys. Rev. B **38**, 11 068 (1988); M. Przybylski, I. Kaufmann, and U. Gradmann, Phys. Rev. B **40**, 8631 (1989); T. Shinjo, Surf. Sci. Rep. **12**, 49 (1991).
[10] L. Niesen, A. Mugarza, M. F. Rosu, R. Coehoorn, R. M. Jungblut, F. Roozeboom, A. Q. R. Baron, A. I. Chumakov, and R. Rüffer, Phys. Rev. B **58**, 8590 (1998).
[11] R. Röhlsberger, J. Bansmann, V. Senz, K. L. Jonas, A. Bettac, O. Leupold, R. Rüffer, E. Burkel, and K. H. Meiwes-Broer, Phys. Rev. Lett. **86**, 5597 (2001).
[12] E. Gerdau, R. Rüffer, H. Winkler, W. Tolksdorf, C. P. Klages, and J. P. Hannon, Phys. Rev. Lett. **54**, 835 (1985).
[13] J. B. Hastings, D. P. Siddons, U. van Bürck, R. Hollatz, and U. Bergmann, Phys. Rev. Lett. **66**, 770 (1991).
[14] U. van Bürck, D. P. Siddons, J. B. Hastings, U. Bergmann, and R. Hollatz, Phys. Rev. B **46**, 6207 (1992).
[15] J. P. Liu, C. P. Luo, Y. Liu, and D. J. Sellmyer, Appl. Phys. Lett. **72**, 483 (1998).
[16] C. M. Kuo, P. C. Kuo, H. C. Wu, Y. D. Yao, and C. H. Lin, J. Appl. Phys. **85**, 4886 (1999).
[17] R. Rüffer and A. I. Chumakov, Hyperfine Interact. **97/98**, 589 (1996).
[18] S. Jeong, Y. Hsu, D. E. Laughlin, and M. E. McHenry, IEEE Trans. Magn. **37**, 1299 (2001).
[19] The formalism presented here is not restricted to an in-plane magnetization. For the general case and an extension to out-of-plane components, see, e.g., [11].
[20] J.-U. Thiele, L. Folks, M. F. Toney, and D. K. Weller, J. Appl. Phys. **84**, 5686 (1998).
[21] Values quoted in the literature are $A_s = 2.8 \times 10^{-6}$ erg/cm [6] and $A_s = 1.9 \times 10^{-6}$ erg/cm [22].
[22] M. B. Stearns, in *Magnetic Properties of Metals*, edited by H. P. J. Wijn, Landolt-Börnstein, New Series, Group III, Vol. 19a (Springer, Berlin, 1986).
[23] G. S. D. Beach, A. E. Berkowitz, V. G. Harris, F. T. Parker, B. Ramadurai, and D. J. Smith, J. Appl. Phys. **91**, 7526 (2002).
[24] K. Koike and T. Furukawa, Phys. Rev. Lett. **77**, 3921 (1996).